Microelectronics Journal 153 (2024) 106402

Contents lists available at ScienceDirect

Microelectronics Journal

journal homepage: www.elsevier.com/locate/mejo

Miniaturized bandpass filter with ultrawide-stopband and high selectivity using glass-based IPD technology

Jianye Wang, Yazi Cao [*], Wei Wu [**], Gaofeng Wang [***]

MOE Engineering Research Center of Smart Microsensors and Microsystems, School of Electronics and Information, Hangzhou Dianzi University, Hangzhou, Zhejiang, 310018, China

A R T I C L E I N F O

Keywords:
Bandpass filter (BPF)
Transmission zero
High selectivity
Wide stopband
Impedance inverter

A B S T R A C T

A miniaturized bandpass filter (BPF) with ultrawide-stopband and high selectivity performance is proposed by virtue of glass-based integrated passive devices (IPD) technology. The proposed BPF consists of two modified second-order units and an impedance inverter. In the modified second-order units, two capacitors are added to the traditional second-order Chebyshev bandpass filter, which can generate two additional transmission zeros locating in the lower and upper bands, respectively. Moreover, these two modified second-order units are cascaded to improve the selectivity and achieve the ultrawide-stopband of the proposed BPF. In addition, the cascaded impedance inverter is introduced to further improve impedance matching of the proposed BPF. The proposed BPF is fabricated using glass-based IPD technology and measured by on-wafer probing. The fabricated BPF has a compact size of 1.0 mm × 1.0 mm × 0.35 mm. The measured results show that the fabricated BPF can cover the wide operating band from 3.3 GHz to 5.0 GHz with an insertion loss of 1.4 dB, a return loss better than 17.5 dB in the passband, and an upper stopband suppression better than 21.6 dB up to 43.5 GHz (10.48f_0). In addition, the fabricated BPF can achieve a good frequency selectivity with a rectangular coefficient of 1.33. The simulated and measured results exhibit good agreements.

1. Introduction

BANDPASS filters (BPFs) are indispensable components in wireless communication systems. It is highly in demand that the BPFs can exhibit compact size, high selectivity, and wide stopband [1–18]. There are many efforts on this topic using different technologies, such as GaAs-based [1–6], high resistivity silicon [7–9], and glass-based [10–13].

In [1], independently controllable transmission zeros were introduced on both sides of the passband by using LC resonators to achieve high selectivity. In Ref. [2], based on the Chebyshev filter structure, a pole-zero was implemented to generate a notch pattern, thereby enhancing the sharp-drop capability. In Ref. [10], for the purpose of low insertion loss and high selectivity, the BPF using a stacked bilayer structure on glass process was introduced, which was, however, unable to achieve a broad upper stopband region. To obtain BPFs with wide stopbands, some previous efforts have been exerted in Refs. [3–5]. In Ref. [3], a new π-section has been introduced to realize wide stopband. In Ref. [4], high selectivity and ultra-wide upper stopband were achieved by introducing source-load coupling and Pi-section circuit. In Ref. [7], By generating multiple transmission zeros, high roll-off rates at the passband edge and good rejection in ultra-wide stopband were achieved on HRS technology. However, the insertion loss was not good. In Ref. [5], the design employed a stepped-impedance multimode resonator and achieved a high rejection to fourth/fifth order of the passband, but its size was not compact.

In this work, a miniaturized BPF with ultrawide-stopband and high selectivity performance is proposed by virtue of glass-based IPD technology. High selectivity and ultrawide-stopband are achieved by cascading two modified second-order units through one impedance inverter, which can generate four transmission zeros. The proposed BPF is fabricated using a glass IPD process. The performance of the fabricated BPF is competitive compared to the previously reported BPFs.

* Corresponding author.
** Corresponding author.
*** Corresponding author.
E-mail addresses: caoyazi@hdu.edu.cn (Y. Cao), bwu@cynoware.com (W. Wu), gaofeng@hdu.edu.cn (G. Wang).

https://doi.org/10.1016/j.mejo.2024.106402
Received 9 August 2024; Received in revised form 4 September 2024; Accepted 5 September 2024
Available online 12 September 2024
1879-2391/© 2024 Elsevier Ltd. All rights reserved, including those for text and data mining, AI training, and similar technologies.

2. Proposed design and analysis

The proposed BPF consists of two modified second-order units and one impedance inverter. The circuit topology of the proposed BPF with nine capacitors and four inductors is shown in Fig. 1.

2.1. Modified second-order units

A simple circuit of the conventional second-order Chebyshev filter is shown in Fig. 2(a). It consists of two resonators, including series LC resonator with L_2 and C'_4 in the main branch and parallel LC resonator with L_1 and C_2 in the shunt branch. Based on Fig. 2(a), a modified second-order unit is introduced to generate an additional pair of transmission zeros near the passband, as shown in Fig. 2(b). In this modified second-order unit, C_3 is connected in parallel with L_2 and then in series with C'_4 in the main branch, and C_1 is connected in series with L_1 and in parallel with C_2 in the shunt branch. As the simulated results shown in Fig. 2(c), the conventional second-order unit without C_1 and C_3 cannot generate any transmission zeros, while the modified second-order unit with C_1 and C_3 can generate two transmission zeros locating in the lower and upper bands respectively.

To analyze how the transmission zeros are generated by the (first) modified second-order unit, the ABCD matrix of its two ports network can be obtained as

$$\begin{bmatrix} A & B \\ C & D \end{bmatrix} = \begin{bmatrix} 1 & 0 \\ Y_{l1} & 1 \end{bmatrix} \begin{bmatrix} 1 & Z_{l1} \\ 0 & 1 \end{bmatrix} = \begin{bmatrix} 1 & Z_{l1} \\ Y_{l1} & Y_{l1}Z_{l1}+1 \end{bmatrix} \tag{1}$$

with

$$Y_{l1} = \frac{1}{\left(j\omega L_1 + \frac{1}{j\omega C_1}\right)} + j\omega C_2 = \frac{j\omega(C_1 + C_2 - \omega^2 L_1 C_1 C_2)}{1-\omega^2 L_1 C_1}$$

$$Z_{l1} = \frac{1}{j\omega C_3 + \frac{1}{j\omega L_2}} + \frac{1}{j\omega C'_4} = \frac{(1-\omega^2 L_1 C_1)(1-\omega^2 L_2 C_3 - \omega^2 L_2 C'_4)}{j\omega C'_4(1-\omega^2 L_1 C_1)(1-\omega^2 L_2 C_3)}$$

where ω is the transmission frequency of the filter, $C_1 = 0.875$ pF, $C_2 = 0.423$ pF, $C_3 = 0.270$ pF, $C'_4 = 0.300$ pF, $L_1 = 4.476$ nH, and $L_2 = 2.012$ nH. The S-parameter S_{12} is related to the ABCD matrix as follows:

$$S_{12} = S_{21} = \frac{2(AD-BC)}{A + B/Z_0 + CZ_0 + D} \tag{2}$$

When $S_{12} = 0$, the values of ω are the transmission zeros, which can be determined as

$$\begin{cases} \omega_1 = \sqrt{\dfrac{1}{L_1 C_1}} \\ \omega_2 = \sqrt{\dfrac{1}{L_2 C_3}} \end{cases} \tag{3}$$

From (3), the two transmission zeros (TZ_1, TZ_2) can be obtained as

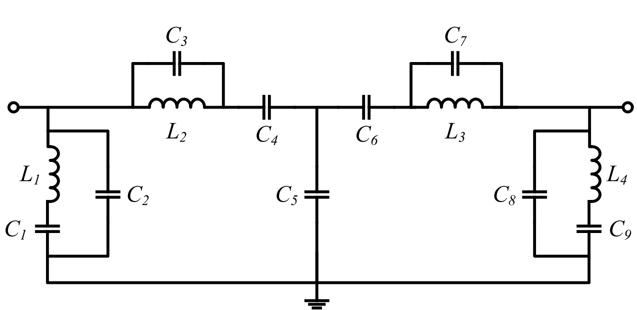

Fig. 1. Schematic of the proposed BPF.

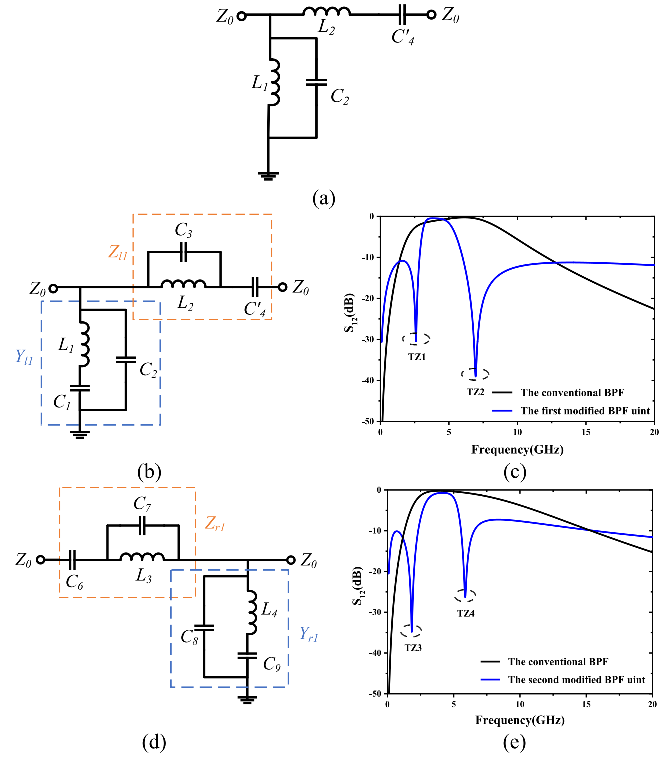

Fig. 2. (a) Conventional second-order Chebyshev filter. (b) Circuit topology of the first modified second-order unit. (c) Simulated S_{12} of the first modified second-order unit. (d) Circuit topology of the second modified second-order unit. (e) Simulated S_{12} of the second modified second-order unit.

2.54 GHz and 6.83 GHz, respectively.

A second modified second-order unit is shown in Fig. 2(d), which has a mirror topology of the first modified second-order unit in Fig. 2(b), with different element values. The second modified second-order unit can also result in two transmission zeros (TZ_3, TZ_4), which may be at different locations from TZ_1 and TZ_2 of the first modified second-order unit. Herein, $C_6 = 1.456$ pF, $C_7 = 0.871$ pF, $C_8 = 0.810$ pF, $C_9 = 4.661$ pF, $L_3 = 0.821$ nH, and $L_4 = 1.594$ nH. The two transmission zeros (TZ3, TZ4) are obtained as 1.85 GHz and 5.95 GHz, respectively.

The circuits in Fig. 2(b) and (d) are both based on the topology of conventional second-order Chebyshev filter in Fig. 2 (a). In this design, the conventional second-order Chebyshev filter in Fig. 2 (a) has band-pass characteristic, the passband position is the same, and the device values in Fig. 2 (b) and 2(d) are adjusted only to fine-tune the position of the transmission zeros (TZs). Therefore, the structure of the two is similar, and the frequency response can be similar in a certain range.

Fig. 3(a)and (b) show the variation of the two TZs (TZ_1, TZ_2), which do not affect each other and are determined by L_1, C_1 and L_2, C_3, respectively. In Fig. 3(a), when C_1 is unchanged, TZ_1 moves closer the passband with the decrease of L_1, and the selectivity is enhanced. When L_1 is unchanged, TZ_1 moves closer the passband with the decrease of C_1, and the selectivity is enhanced. In Fig. 3(b), when C_3 is unchanged, TZ_2 moves closer the passband with the increase of L_2, and the selectivity is enhanced. When L_2 is unchanged, TZ_2 moves closer to the passband with the increase of C_3, and the selectivity is enhanced. Similarly, Fig. 3(c) and (d) show the variation of two TZs (TZ_3, TZ_4) that do not affect each other and are determined by L_4, C_9 and L_3, C_7, respectively.

2.2. Impedance K-inverter

In [14–16], impedance inverters are employed to improve the BPF performance, but all of them are based on the transmission line designs.

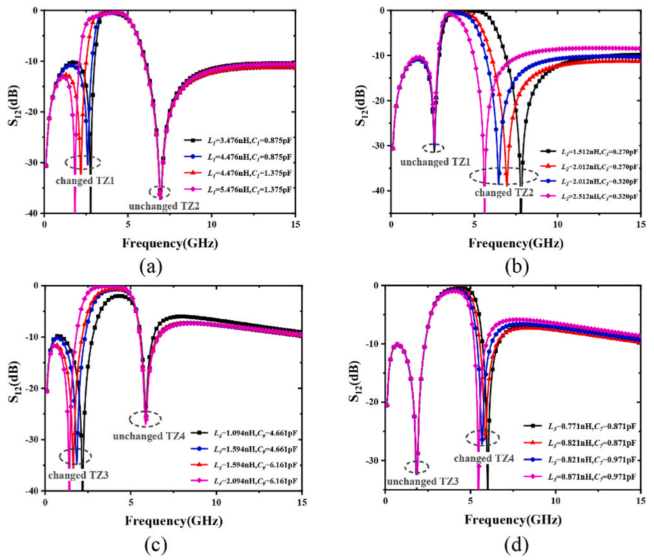

Fig. 3. (a) First modified second-order unit with changed TZ_1 and unchanged TZ_2(C_2 = 0.423 pF, C_3 = 0.270 pF, C'_4 = 0.300 pF and L_2 = 2.012 nH). (b) First modified second-order unit with unchanged TZ_1 and changed TZ_2(C_1 = 0.875 pF, C_2 = 0.423 pF, C'_4 = 0.300 pF and L_1 = 4.476 nH). (c) Second modified second-order unit with changed TZ_3 and unchanged TZ_4(C_6 = 1.456 pF, C_7 = 0.871 pF, C_8 = 0.810 pF and L_3 = 0.821 nH). (d) Second modified second-order unit with unchanged TZ_3 and changed TZ_4(C_6 = 1.456 pF, C_8 = 0.810 pF, C_9 = 4.661 pF and L_4 = 1.594 nH).

There are various ways to implement impedance inverters, depending on the size requirements and the operating frequency. Herein, the impedance K-inverter is introduced based on the lumped LC approach by cascading the two modified second-order units, which can improve their impedance matching. The proposed impedance K-inverter cascading the two modified second-order units (BPFs) is as shown in Fig. 4(a).

As shown in Fig. 4(b), this impedance K-inverter consists of lumped elements series -C_a and shunt C_b. The input impedance Z_{in} and the load impedance Z_L at both ends of the impedance K-inverter satisfy the following relationship:

$$\begin{cases} Z_{in} = \left(\dfrac{1}{j\omega C_b + \dfrac{1}{Z_L}}\right) + \dfrac{1}{j\omega(-C_a)} \\ Z_{in} = \dfrac{K^2}{Z_L} = \dfrac{K^2}{\mathrm{Re}(Z_L) + j\mathrm{Im}(Z_L)} = \dfrac{K^2}{R_L + jX_L} \end{cases} \tag{4}$$

where ω is the angular frequency, K is the characteristic impedance of the impedance inverter, R_L is the real part of Z_L, X_L is the imaginary part of Z_L.

From (4), the expressions for -C_a and C_b can be obtained as

$$\begin{cases} -C_a = \dfrac{|Z_L|^2}{\omega K\left(KX_L - \sqrt{|Z_L|^4 - K^2R_L^2}\right)} \\ C_b = \dfrac{X_L}{\omega|Z_L|^2} + \dfrac{\sqrt{|Z_L|^4 - K^2R_L^2}}{\omega K|Z_L|^2} \end{cases} \tag{5}$$

As shown in Fig. 5(a), the proposed filter is composed of two modified second-order units (Unit_L, Unit_R) and one impedance K-inverter. The K-inverter is utilized to cascade Unit_L and Unit_R, which can improve the impedance matching of these two units. The capacitance value of -C_a is a negative value, which will be absorbed by the resonance in Unit_L. C'_4 and -C_a are combined into one capacitor C_4.

Fig. 5(b) and (c) show the changes of the two TZs near the sides of the passband, which are independently controlled by L_1, C_1, and L_3, C_7, respectively. As L_1 or C_1 increases, TZ_1 moves away from the passband in Fig. 5(b). As L_3 or C_7 decreases, TZ_4 will move away from the passband in Fig. 5(c). Therefore, in a certain range, the proposed BPF can control the center frequency and bandwidth by adjusting the device values of L_1, C_1, L_3 and C_7. When two transmission zeros (TZ_1, TZ_4) are close to each other, the bandwidth decreases, and vice versa, the bandwidth increases. When the two transmission zeros (TZ_1, TZ_4) move in the same direction, the center frequency of the filter passband moves accordingly.

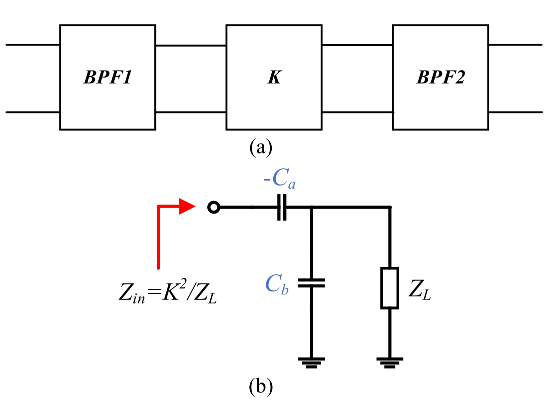

Fig. 4. (a) Configuration of the proposed BPF with impedance K-inverter. (b) Circuit schematic of impedance K-inverter.

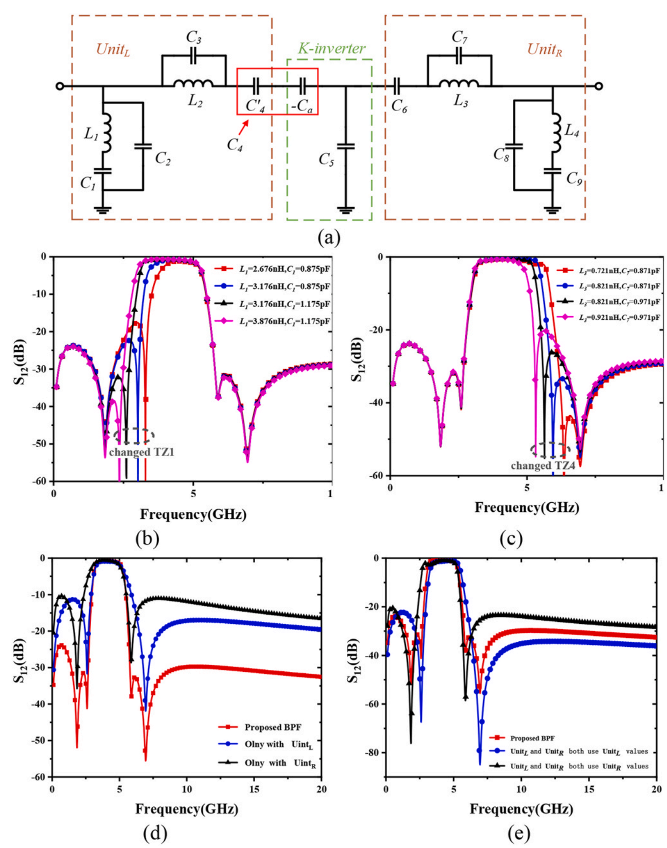

Fig. 5. Proposed IPD BPF. (a) Cascading circuit schematic. (b) With changed TZ_1(C_2 = 0.423 pF, C_3 = 0.270 pF, C_4 = 0.453 pF, C_5 = 0.353 pF, C_6 = 1.456 pF, C_7 = 0.871 pF, C_8 = 0.810 pF, C_9 = 4.661 pF, L_2 = 2.012 nH, L_3 = 0.821 nH, and L_4 = 1.594 nH). (c) With changed TZ_4(C_1 = 0.875 pF, C_2 = 0.423 pF, C_3 = 0.270 pF, C_4 = 0.453 pF, C_5 = 0.353 pF, C_6 = 1.456 pF, C_8 = 0.810 pF, C_9 = 4.661 pF, L_1 = 4.476 nH, L_2 = 2.012 nH, and L_4 = 1.594 nH). (d) Simulated S_{12} of only with Unit_L or Unit_R. (e) Simulated S_{12} of Unit_L or Unit_R with the same values.

Compared with the red curve in Fig. 5(d) in this paper, as shown in the blue curve in Fig. 5(d), the proposed BPF with only Unit$_L$ can only generate two transmission zeros (TZs), the roll-off at the high frequency side of the passband is not sharp, and the suppression ability of the upper and lower stopband is poor. Same with the proposed BPF with only Unit$_R$

In Fig. 5(e), if the component values of Unit$_L$ and Unit$_R$ correspondingly equal, the circuit only can generate two TZs, the position of one transmission zero will be far away from the passband, which cannot improve the selectivity. Therefore, the component values of Unit$_L$ and Unit$_R$ are different, the proposed BPF can generate four transmission zeros at different locations to further improve high selectivity and ultra-wide stopband.

Based on the above analysis, the final circuit parameters are chosen as follows: $C_1 = 0.875$ pF, $C_2 = 0.423$ pF, $C_3 = 0.270$ pF, $C_4 = 0.453$ pF, $C_5 = 0.353$ pF, $C_6 = 1.456$ pF, $C_7 = 0.871$ pF, $C_8 = 0.810$ pF, $C_9 = 4.661$ pF, $L_1 = 4.476$ nH, $L_2 = 2.012$ nH, $L_3 = 0.821$ nH, and $L_4 = 1.594$ nH. Fig. 6(a) presents the simulated S-parameters based on the proposed BPF circuit schematic. It can be observed that the final circuit can generate four TZs including two transmission zeros (TZ$_1$, TZ$_3$) in the lower band and two (TZ$_2$, TZ$_4$) in the higher band. It can greatly improve the selectivity in the sidebands and extend the stopband frequency range. The three-dimensional (3D) layout view of the proposed BPF is shown in Fig. 6(b).

3. Fabrication and measurement

The proposed BPF is fabricated using glass-based integrated passive devices (IPD) technology. Fig. 7(a) shows the cross-section view of the glass-based IPD technology. The glass substrate has a thickness of 330 μm, a relative dielectric constant ε_r of 4.4, and a loss tangent of 0.0073. This technology includes three thick metal (Cu) layers, i.e., M1, TM1, and TM2 with thicknesses of 0.2 μm, 5 μm and 5 μm, respectively. The inductors are fabricated on layer TM1. The MIM capacitors are fabricated on layers M1 and TM2, which are separated by a dielectric layer with a relative dielectric constant of 6.8. Compared with silicon-based technology, the BPF based on glass-based IPD technology can achieve low insertion loss because of its lower substrate loss. Fig. 7(b) shows the layout of the fabricated BPF, which has a size of 1.0 × 1.0 mm^2 (0.029 × 0.029 λ_g^2).

The EM simulation is performed by UltraEM [19]. This BPF is measured by on-wafer probing using the Keysight N5247A vector network analyzer. The results of EM simulation and measurement are shown in Fig. 7(c). From the measured results, the center frequency f_0 is 4.15 GHz, the 3 dB fractional bandwidth is 63.37 %, the insertion loss within the passband is less than 1.4 dB, and the return loss is greater than 17.5 dB. In the lower stopband, a 20-dB rejection is achieved from DC to 2.73 GHz, and the upper stopband suppression is better than 21.6 dB from 6.17 GHz to 43.5 GHz, showing a very wide stopband. Good agreement between the simulated and measured results is clearly observed.

Table 1 shows the comparison between this work and previously reported works. The proposed BPF has a more compact size yet achieve a wider stopband by comparison to those from Refs. [1,6,7,11]. Moreover, the proposed BPF has lower insertion loss compared to those from Refs. [1,3,6,11]. In conclusion, this proposed filter can simultaneously exhibit

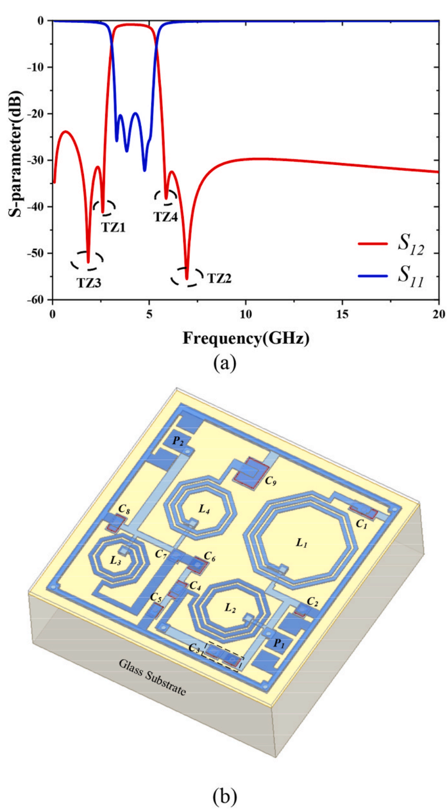

Fig. 6. Proposed IPD BPF. (a) Simulated S-parameters of the proposed circuit schematic. (b) 3D view of layout.

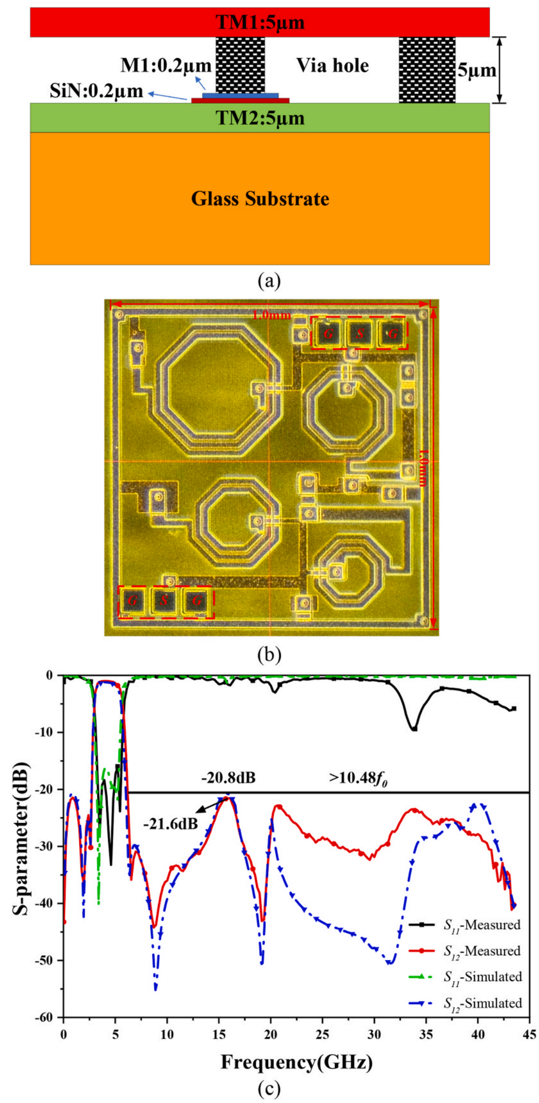

Fig. 7. (a) Stack-up of the glass-based IPD technology. (b) Die photograph of the fabricated BPF. (c) Simulated and measured results of the fabricated BPF.

Table 1
Comparison of the proposed BPF with other recent works.

Ref.	f_0(GHz)	Rej(dB)/Stopband	IL (dB)	Size (λ_g^2)	Tech
[1]	3.58	26.2/2.79$^+$ f_0	1.67	0.028 × 0.016$^+$	GaAs
[3]	3	20/34.6 f_0	1.77	0.059 × 0.021	GaAs
[6]	3.5	14/1.71$^+$ f_0	2	0.040 × 0.041	GaAs
[7]	3.75	20/8.3 f_0	1.50	0.047 × 0.030$^+$	HRS
[11]	8.6	15/1.63$^+$ f_0	2.1	0.520 × 0.250	Glass
This work	4.15	21.6/10.48 f_0	1.4	0.029 × 0.029	Glass

λ_g: The guide wavelength at f_0; HRS: High Resistivity Silicon. +: Calculate from the data given.

merits of compact size, low insertion loss, high selectivity, and high wide stopband.

4. Conclusion

In this work, a miniaturized bandpass filter based on glass IPD technology has been proposed. The proposed BPF consists of two modified second-order units and an impedance K-inverter. Two modified second-order units can generate four transmission zeros for high selectivity and ultra-wide stopband. To further improve the performance of the proposed BPF, two modified second-order units are cascaded by the impedance K- inverter. From the measured results, one can observe that the proposed BPF can achieve a low insertion loss of 1.4 dB, a rectangular coefficient of 1.33, and an upper stopband suppression better than 21.6 dB up to 43.5 GHz (10.48f_0). The proposed BPF exhibits merits of miniaturized size, low insertion loss, ultra-wide stopband, and high selectivity, which make it applicable for 5G RF front-end applications.

Author statement

Dear Editor and Reviews, Please find submitted the revised version of ID MEJ-D-24-00999, entitled “Miniaturized Bandpass Filter with Ultrawide-Stopband and High Selectivity using Glass-Based IPD Technology”, co-authored by J. Wang, W. Wu, G. Wang, and me. Here is our Author Statement to agree and publish our paper to MEJ.

Declaration of competing interest

The authors declare that they have no known competing financial interests or personal relationships that could have appeared to influence the work reported in this paper.

Data availability

No data was used for the research described in the article.

Acknowledgements

This work was supported by National Natural Science Foundation of China under Grants 92373202 and 62141409, Zhejiang Provincial Natural Science Foundation of China under Grant No. LQ24F010010, National Key Research and Development Program of China under Grant 2019YFB2205003, and Zhejiang Provincial Key Research & Development Project under Grant 2021C01041.

References

[1] Y. Xu, Y. Wu, H. Wu, Y. Yang, W. Wang, Wideband high selectivity filter chips with adjustable bandwidth based on IPD technology, IEEE Transactions on Circuits and Systems II: Express Briefs 69 (11) (Nov. 2022) 4273–4277.
[2] Ji-Hu Li, Cong Wang, Luqman Ali, Xiao Tan, Wei Yu-Chen, Ho-Kun Sung, Zhi-Qiang Gao, Shan-Shan Xu, Yang Li, Design and optimization of GaAs-based thin film integrated passive device bandpass filters for 5G communications, Microelectron. J. 139 (2023) 105913.
[3] Y. Jiang, et al., Bandpass filter with ultra-wide upper stopband on GaAs IPD technology, IEEE Transactions on Circuits and Systems II: Express Briefs 69 (2) (Feb. 2022) 389–393.
[4] X.-H. Luo, et al., A miniaturized on-chip BPF with ultrawide stopband based on lumped Pi-section and source-load coupling, IEEE Microw. Wireless Compon. Lett. 29 (8) (Aug. 2019) 516–519.
[5] Y.-P. Lyu, Y.-J. Zhou, L. Zhu, C.-H. Cheng, Compact and high-order on-chip wideband bandpass filters on multimode resonator in integrated passive device technology, IEEE Electron. Device Lett. 43 (2) (Feb. 2022) 196–199.
[6] W. Chen, Y. Wu, Y. Yang, W. Wang, IPD-based miniaturized wideband bandpass filter with frequency-dependent complex source and load, IEEE Trans. Plasma Sci. 49 (3) (March 2021) 1115–1120.
[7] J. Zhang, J.-X. Xu, C. Yao, X.Y. Zhang, Miniaturized high-selectivity high-resistivity-silicon IPD bandpass filter based on multiple transmission paths, IEEE Electron. Device Lett. 45 (4) (April 2024) 534–537.
[8] Y. Qi, Y. Cao, B. Yuan, S. Chen, K. Zhang, G. Wang, Compact on-chip dual-band bandpass filter with wide out-of-band suppression based on hybrid coupling technique, Microelectron. J. 151 (2024) 106304.
[9] B. Xu, Y. Cao, B. Yuan, S. Chen, G. Wang, Compact IPD bandpass filters based on coupling-enhanced transformer and metamaterial lowpass structure, IEEE Trans. Compon. Packag. Manuf. Technol. (2024), https://doi.org/10.1109/TCPMT.
[10] H. Ma, Z. Hu, D. Yu, A low-loss bandpass filter with stacked double-layer structure using glass-based integrated passive device technology, IEEE Electron. Device Lett. 44 (7) (July 2023) 1216–1219.
[11] W. Zhang, J. Gu, L. Li, X. Li, Through-glass-via based microstrip band-pass filters fabricated with wafer-level low-melting-point alloy micro-casting, IEEE Electron. Device Lett. 41 (7) (July 2020) 1106–1109.
[12] J. Tang, H. Liu, Y. Yang, Compact wide-stopband dual-band balanced filter using an electromagnetically coupled SIR pair with controllable transmission zeros and bandwidths, IEEE Transactions on Circuits and Systems II: Express Briefs 67 (11) (Nov. 2020) 2357–2361.
[13] J. Xin, Y. Cao, H. Li, M. Xu, G. Wang, A novel design method for wideband bandpass filters with fewer inductors, Microelectron. J. 151 (2024) 106300.
[14] A. Barakat, R.K. Pokharel, Low-pass filtering admittance inverter for high out-of-band rejection millimeter-wave on-chip BPF, IEEE Transactions on Circuits and Systems II: Express Briefs 70 (11) (Nov. 2023) 3963–3967.
[15] H. Zhu, X. Zhu, Y. Yang, Q. Xue, Design of wideband third-order bandpass filters using broadside-coupled resonators in 0.13-μm (Bi)-CMOS technology, IEEE Trans. Microw. Theor. Tech. 66 (12) (Dec. 2018) 5593–5604.
[16] G. Chaudhary, Y. Jeong, Frequency tunable impedance matching nonreciprocal bandpass filter using time-modulated quarter-wave resonators, IEEE Trans. Ind. Electron. 69 (8) (Aug. 2022) 8356–8365.
[17] Chenhui Fan, Xiaoxian Liu, Nuo Liu, Yintang Yang, Zhangming Zhu, An effective method to suppress high-order modes of SIW filters with compact size, Microelectron. J. 127 (2022) 105519.
[18] Yi Le, Hongcheng Dong, Guodong Su, Jinsong Zhan, Quan Xing, Jun Liu, A miniaturized and low-loss Q-band SIW bandpass filter based on evanescent-mode in wafer-level packaging process, Microelectron. J. 149 (2024) 106209.
[19] V.2023 UltraEM, Faraday Dynamics, Inc., Hangzhou, Zhejiang, China, 2023.